

METHOD

Open Access



# SURF: integrative analysis of a compendium of RNA-seq and CLIP-seq datasets highlights complex governing of alternative transcriptional regulation by RNA-binding proteins

Fan Chen<sup>1</sup> and Sündüz Keleş<sup>1,2\*</sup>

\*Correspondence:

[keles@stat.wisc.edu](mailto:keles@stat.wisc.edu)

<sup>1</sup>Department of Statistics, University of Wisconsin-Madison, 1220 Medical Sciences Center, 1300 University Avenue, Madison, WI 53706, USA

<sup>2</sup>Department of Biostatistics and Medical Informatics, University of Wisconsin-Madison, K6/446 Clinical Sciences Center, 600 Highland Avenue, Madison, WI 53792-4675, USA

## Abstract

Advances in high-throughput profiling of RNA-binding proteins (RBPs) have resulted in CLIP-seq datasets coupled with transcriptome profiling by RNA-seq. However, analysis methods that integrate both types of data are lacking. We describe SURF, Statistical Utility for RBP Functions, for integrative analysis of large collections of CLIP-seq and RNA-seq data. We demonstrate SURF's ability to accurately detect differential alternative transcriptional regulation events and associate them to local protein-RNA interactions. We apply SURF to ENCODE RBP compendium and carry out downstream analysis with additional reference datasets. The results of this application are browsable at <http://www.statlab.wisc.edu/shiny/surf/>.

**Keywords:** RNA-binding protein, CLIP-seq, RNA-seq, Integrative modeling, Differential analysis, Alternative splicing, Alternative polyadenylation, Transcriptional regulation

## Background

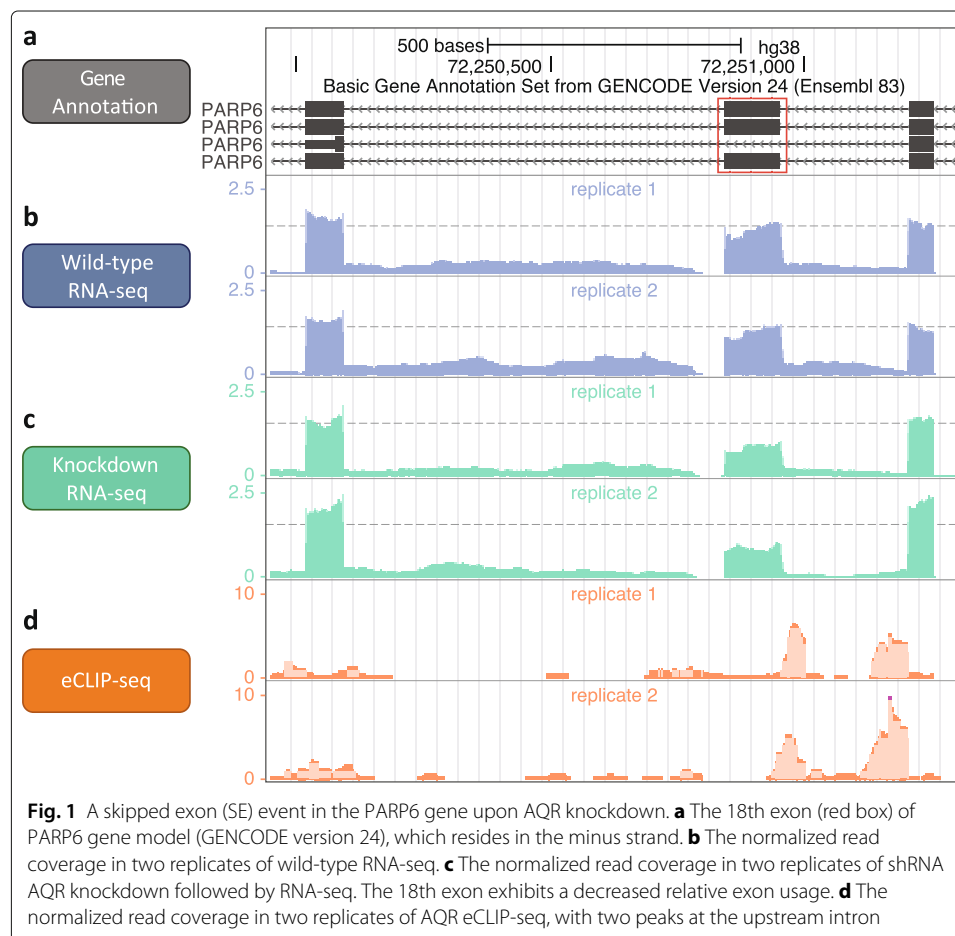
RNA-binding proteins (RBPs) constitute a key class of regulators for post-transcriptional processes such as splicing, polyadenylation, transportation, translation, and degradation of RNA transcripts in eukaryotic organisms [1, 2]. They drive the diversity and complexity of transcriptome and proteome through gene expression regulation at the RNA level with alternative splicing (AS), alternative transcription initiation (ATI), and alternative polyadenylation (APA) [3, 4]. High-throughput sequencing-based assays that quantify protein-RNA interactions (e.g., ultraviolet cross-linking immunoprecipitation followed by high-throughput sequencing (CLIP-seq)) have recently matured and revealed a rich repertoire of RBP profiles in cell lines and tissues [5–7]. When coupled with the analysis of RNA-seq experiments across multiple conditions to elucidate alternative transcriptional



© The Author(s). 2020 **Open Access** This article is licensed under a Creative Commons Attribution 4.0 International License, which permits use, sharing, adaptation, distribution and reproduction in any medium or format, as long as you give appropriate credit to the original author(s) and the source, provide a link to the Creative Commons licence, and indicate if changes were made. The images or other third party material in this article are included in the article's Creative Commons licence, unless indicated otherwise in a credit line to the material. If material is not included in the article's Creative Commons licence and your intended use is not permitted by statutory regulation or exceeds the permitted use, you will need to obtain permission directly from the copyright holder. To view a copy of this licence, visit <http://creativecommons.org/licenses/by/4.0/>. The Creative Commons Public Domain Dedication waiver (<http://creativecommons.org/publicdomain/zero/1.0/>) applies to the data made available in this article, unless otherwise stated in a credit line to the data.

regulation (ATR) events of classes AS, ATI, and APA, these studies can suggest specific roles for RBPs in different types of events such as exon skipping (SE), alternative 3' (A3SS) or 5' (A5SS) splicing, intron retention (RI) within the AS class, alternative first exon (AFE) or alternative 5'UTR (A5U) within the ATI class, and intronic (IAP) or tandem (TAP) alternative polyadenylation within the APA class [8] (Additional file 1: Fig. S1).

The ENCODE (ENCyclopedia of DNA elements) project [9, 10] recently generated eCLIP-seq datasets for 120 and 104 RBPs in human cell lines K562 and HepG2. These datasets were complemented with RNA-seq datasets of the same cell lines under conditions of both wild-type and short hairpin RNA (shRNA) knockdown of the individual RBPs to identify differentially regulated AS, ATI, and APA events (Fig. 1). The initial analysis by the ENCODE project revealed a large set of genomic elements interacting with RBPs and expanded the catalogue of biochemically active elements of the genome [11, 12]. In this paper, we develop a statistical framework that augments the existing analysis by specifically inferring global positioning principles of RBPs with respect to the above eight types of ATR events. Our method, named SURF for *Statistical Utility for RBP Functions*, consists of two analysis and a discovery modules. The first analysis module identifies differential ATR events within AS, ATI, and APA classes by comparing wild-type and shRNA knockdown RNA-seq data, with multiple replicates from each. The second module associates the detected differential ATR events to position-specific



eCLIP-seq signals, thereby dissecting global positioning principles of protein-RNA interactions in different types of ATR events. The discovery module of SURF queries existing reference transcriptome databases, i.e., the genotype-tissue expression (GTEx) project [13] and the Cancer Genome Atlas (TCGA) program [14], to assess differential activity of ATR-specific transcript targets of RBPs between normal tissue and the relevant tumor samples.

A number of computational tools exist for detecting differential alternative splicing from RNA-seq data across two conditions (e.g., MISO [15], MATS [16], DSGseq [17], MAJIQ [18], and rMATS [19]). These methods circumvent the challenges of direct transcriptome quantification imposed by the short read sequencing by evaluating differential ATR for each unit consisting of a cassette exon and two flanking exons. They directly test for differential ATR events of types SE, A3SS, A5SS, and RI, but not ATI and APA [20–22]. This is in contrast to methods such as Cufflinks [23], DiffSplice [24], SplicingCompass [25], and rSeqDiff [26], which operate at the isoform level. While methods that operate on isoforms test for combined effects of AS, ATI, and APA, the methods in the former category are generally more suited for investigating effects of RBPs on individual ATR events. A powerful alternative and a compromise between the two, as demonstrated by [27], is detecting alternative exon usage, irrespective of the type of ATR event the exon specifies (e.g., DEXSeq [28]). While usage-based method DEXSeq that focuses on “bins” [27] works well in conjunction with many different “unit” definitions (e.g., exons, sub-exonic bins, full length transcripts as “bins”), it does not delineate ATR event types and requires laborious inspection to classify bins into specific event types. The first module of SURF addresses this critical shortcoming by unifying differential ATR detection and generalizing DEXSeq to directly detect explicit types of AS, ATI, and APA events. Differential ATR detection by SURF exhibited superior performance to simple ways of translating DEXSeq usage inference into explicit types of AS, ATI, and APA events and rMATS, which is the only existing method that accommodates replicates within conditions and directly tests for differential ATR of AS events.

De novo sequence analysis of SURF-detected global positioning preferences of regions where eCLIP-seq signals associated with differential ATR event classes AS, ATI, and APA yielded sequence motif multi-modalities of several RBPs in regulating different ATR event types. Further evaluation of these regions revealed a significant enrichment of somatic mutations from both the International Cancer Genome Consortium (ICGC) [29, 30] and TCGA. In addition, analysis of SURF-identified target transcripts of RBPs for their transcriptome activity in normal GTEx versus adult acute myeloid leukemia (LAML) samples from TCGA detected a significant general shift in the activities of groups of transcripts affected by RBP-specific ATR events. These RBPs included both components of spliceosome such as AQR and SF3B4, as well as more specific RBPs such as FXR1 and PUM1. SURF is implemented in R [31] and is publicly available at <https://github.com/keleslab/surf> [32]. The results of the ENCODE data analysis are available through a shiny app at <http://www.statlab.wisc.edu/shiny/surf/>.

## Results

### SURF framework

SURF is designed for large-scale analysis of RBP CLIP-seq and RNA-seq data and includes analyses and discovery modules (Fig. 2). A key input to SURF is genome annotation from

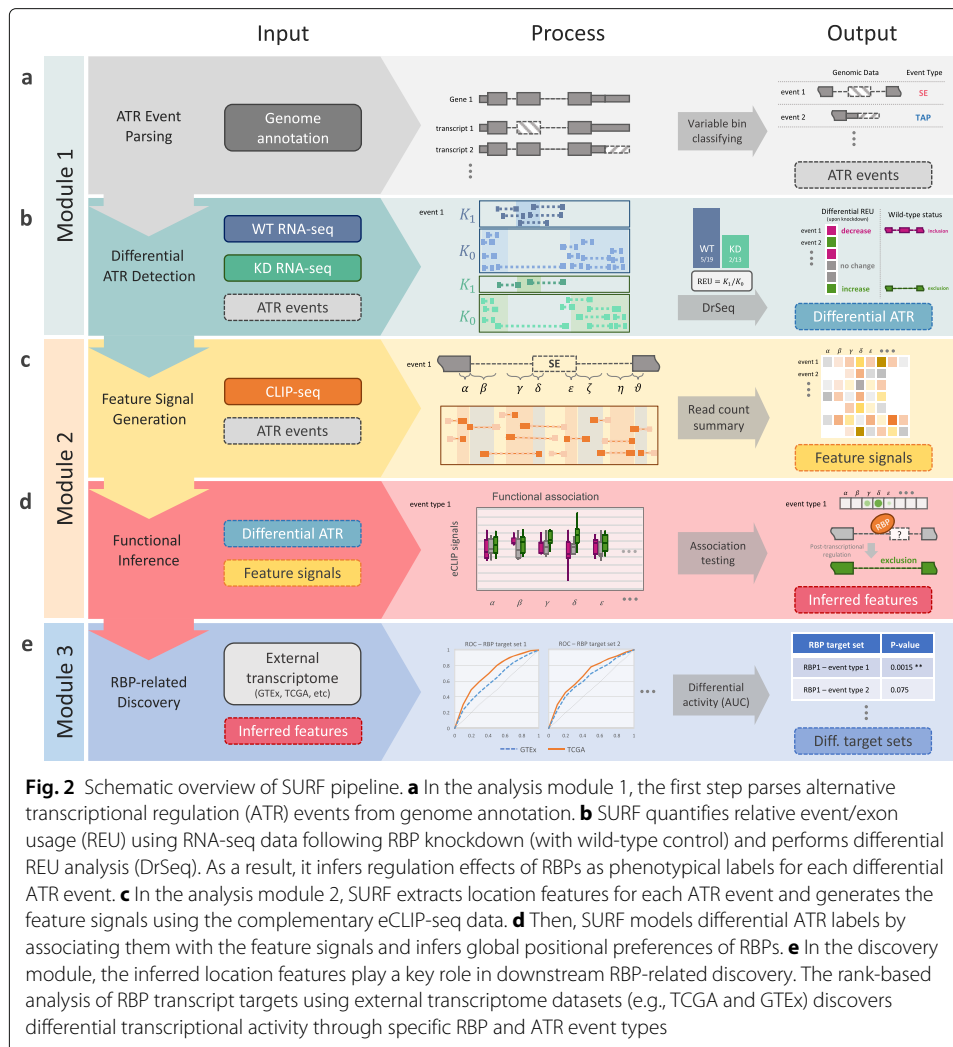


**Fig. 2** Schematic overview of SURF pipeline. **a** In the analysis module 1, the first step parses alternative transcriptional regulation (ATR) events from genome annotation. **b** SURF quantifies relative event/exon usage (REU) using RNA-seq data following RBP knockdown (with wild-type control) and performs differential REU analysis (DrSeq). As a result, it infers regulation effects of RBPs as phenotypical labels for each differential ATR event. **c** In the analysis module 2, SURF extracts location features for each ATR event and generates the feature signals using the complementary eCLIP-seq data. **d** Then, SURF models differential ATR labels by associating them with the feature signals and infers global positional preferences of RBPs. **e** In the discovery module, the inferred location features play a key role in downstream RBP-related discovery. The rank-based analysis of RBP transcript targets using external transcriptome datasets (e.g., TCGA and GTEx) discovers differential transcriptional activity through specific RBP and ATR event types

which SURF parses out all the eight types of ATR events, namely SE, RI, A3SS, A5SS, AFE, A5U, IAP, and TAP (Fig. 2a and Additional file 1: Fig. S2). The parsing procedure utilizes the notion of *variable* exons (or sub-exons) [33] defined as parts of an exon that are in the gene model but are absent in one or more transcripts of the gene. Variable sub-exons of a given transcript can be clustered into mutually exclusive units, as described in the “Materials and methods” section (Additional file 1: Fig. S3), such that each is annotated with a unique ATR event type through a “decision tree” (Additional file 1: Fig. S4). The analysis modules operate on these events, which we also interchangeably refer to as *event body*.

#### Analysis module 1: detecting differential ATR events

We extended the DEXSeq framework to detect differential ATR events of all the eight types by “DrSeq” for *differential regulation* using RNA-seq. Specifically, DrSeq administers the relative exon usage (REU) to characterize any type of AS, ATI, and APA events by detecting differences between the experimental conditions, i.e., wild-type versus knockdown RNA-seq data (Fig. 2b). The REU is defined as the ratio of count of reads overlapping the event body,  $K_1$ , over the count of those reads residing in the other exonic

regions of the same gene,  $K_0$ , and is computed as  $K_1/K_0$  (Fig. 2b). For the  $i$ th event in the  $j$ th sample,  $K_{ijl}$  denotes either the read count on the event body ( $l = 1$ ) or the read count of all the other exonic regions of the same gene ( $l = 0$ ). Similar to the DEXSeq formulation [27] for exonic bins, we model  $K_{ijl}$  with a Negative Binomial (NB) distribution as

$$K_{ijl} \sim \text{NB}(\text{mean} = s_j \mu_{ijl}, \text{dispersion} = \alpha_i),$$

where  $s_j$  is the size factor of the  $j$ th sample and adjusts for the sequencing depth, and  $\alpha_i$  is the dispersion parameter for event  $i$ . The mean parameter  $\mu_{ijl}$  is modeled by a log-link function as

$$\log(\mu_{ijl}) = \beta_{g(i)j}^S + \beta_{il}^E + \beta_{i\rho(j)l}^{\text{EC}}, \quad (1)$$

where  $\rho(j)$  is the experimental condition of sample  $j$  (i.e., wild-type or shRNA knock-down) and  $g(i)$  is the gene (group) from which the  $i$ th event originates. Here,  $\beta_{g(i)j}^S$  accounts for the main effect of each sample and provides a gene-specific log-scale overall read count.  $\beta_{il}^E$  is non-zero only when  $l = 1$  due to identifiability constraints; hence, it quantifies the logarithm of REU,  $K_{ij1}/K_{ij0}$ , for the  $i$ th event across all samples regardless of experimental conditions. Finally,  $\beta_{i\rho(j)l}^{\text{EC}}$  captures the effect of the experimental condition on the REU. This model is fit for each ATR event type by pooling across genes, and the differential REU of each event is quantified by testing the REU  $\times$  condition interaction term ( $\beta^{\text{EC}}$ ) in Eq. (1) under the null hypothesis that the event has equal REU across the conditions. The overall false discovery rate (FDR) is controlled with the Benjamini-Hochberg (BH) procedure [34] by pooling over all ATR event types. SURF further quantifies the change in REU for each ATR event in the form of log<sub>2</sub> fold change in REU. As a result, an “increased REU upon RBP knockdown” indicates the exclusion of variable sub-exons under the wild-type condition. Similarly, a “decreased REU upon RBP knockdown” indicates that RBP tends to promote the inclusion of variable sub-exons under the wild-type condition. We remark that this interpretation does not necessarily extend to core components of the spliceosome since these components are likely to interact with every spliced intron at some level regardless of the inclusion or exclusion outcome.

### **Analysis module 2: testing for positional associations**

To infer global positioning preferences of protein-RNA interactions, SURF extracts event-specific *features* representing the potential locations of protein-RNA interactions, within and flanking the event body, as well as additional genomic regions near the constitutive exons (Additional file 1: Fig. S5). Then, the eCLIP-seq reads over these features are aggregated and normalized to adjust for the lengths of the features and the overall sequencing depth of the samples. We refer to these resulting quantities as *feature signals* (Fig. 2c). Next, SURF associates the feature signals to differential ATR events. Specifically, the ATR events are divided into three groups as “increase” (i.e., increased REU upon RBP knockdown), “decrease,” and “no change,” using the DrSeq results. Then, SURF evaluates the feature signals for their association with these labels of ATR events (Fig. 2d). By adapting a generalized linear model, SURF tests marginal association of each feature and outputs a list of genomic regions that define global positioning preferences of the RBP. This module is applied to each RBP-ATR event type combination separately.

***Discovery module: assessing comparative transcriptional activity of RBP targets***

This module leverages public transcriptome data from GTEx and TCGA to address whether transcripts harboring differential ATR events exhibit differential transcriptional activity between different clinical conditions, e.g., normal (GTEx) versus LAML (TCGA). The module first lifts over the SURF-inferred location features to transcript (or gene) level and forms the sets of transcript (or gene) targets of the RBP, while keeping them specific to ATR event types. For example, the transcript targets of SRSF1 through SE regulation (SRSF1-SE) are the set of transcripts with at least one differential ATR event of type SE regulated by SRSF1. We apply an area under the curve (AUC) approach similar to that in [35] to evaluate whether transcriptional activity of the transcript set significantly differs between the normal and tumor samples, for each combination of RBP and event type (Fig. 2e and Additional file 1: Fig. S6). As a result, this module yields key RBPs with “increased” or “decreased” transcriptional activity in tumor samples through specific AS, ATI, and APA events.

Overall, SURF (i) leverages established appealing characteristics of DEXSeq [27] and generalizes it for detecting differential ATR events, (ii) systematically evaluates associations of differential ATR with protein-RNA interactions, and (iii) offers a unique way of further exploring large compendium of expression data with RBP and ATR event-specific transcript sets.

**SURF enables comprehensive detection of differential ATR events**

We evaluated the differential ATR event detection module (DrSeq) of SURF by comparing it to rMATS [19]. The choice of rMATS among the plethora of available methods is reasoned by the fact that it accommodates biological replicates, which we have two per condition, and that it detects differential ATR for individual alternative splicing events as opposed to the differential exon usage in DEXSeq or the local splice variations in MAJIQ (Additional file 1: Fig. S7). We additionally compared DrSeq with the following two simple strategies of mapping DEXSeq’s results to ATR event level. Specifically, we labeled an event as a differential ATR event when (i) at least one of its exonic bins (liberal strategy, DEXSeq-L) or (ii) at least half of its exonic bins (conservative strategy, DEXSeq-C) is/are identified as differentially used by DEXSeq. We evaluated the above strategies using human transcriptome-based simulated data as described in the “Materials and methods” section. We quantified the performance of each method by its realized power and empirical FDR at gene level at target FDR levels of 0.01, 0.05, and 0.1.

The overall results, summarized in Fig. 3a and Additional file 1: Fig. S8, delineated that all count-based methods (DrSeq and two variants of DEXSeq) achieve significantly higher TPR and lower FDR, compared to rMATS, despite detecting comparable number of events (Additional file 1: Fig. S9). Lower power of rMATS is likely due to the fact that rMATS detects only simple splicing events (i.e., excludes ATI and API). For a limited number of simple ATR event types (e.g., SE), however, rMATS has comparable power with count-based methods (yet worse FDR, Additional file 1: Fig. S10). Higher empirical FDR for rMATS (under various signal-to-noise levels, Additional file 1: Fig. S11) can be largely attributed to the fact that rMATS only utilizes the reads nearby the event body and splice junctions, in contrast to the other count-based methods which account for all reads relevant to the genes (Additional file 1: Fig. S12 and Tables S1 and S2). All count-based methods control the FDR similarly, while DrSeq achieves slightly higher power. The key

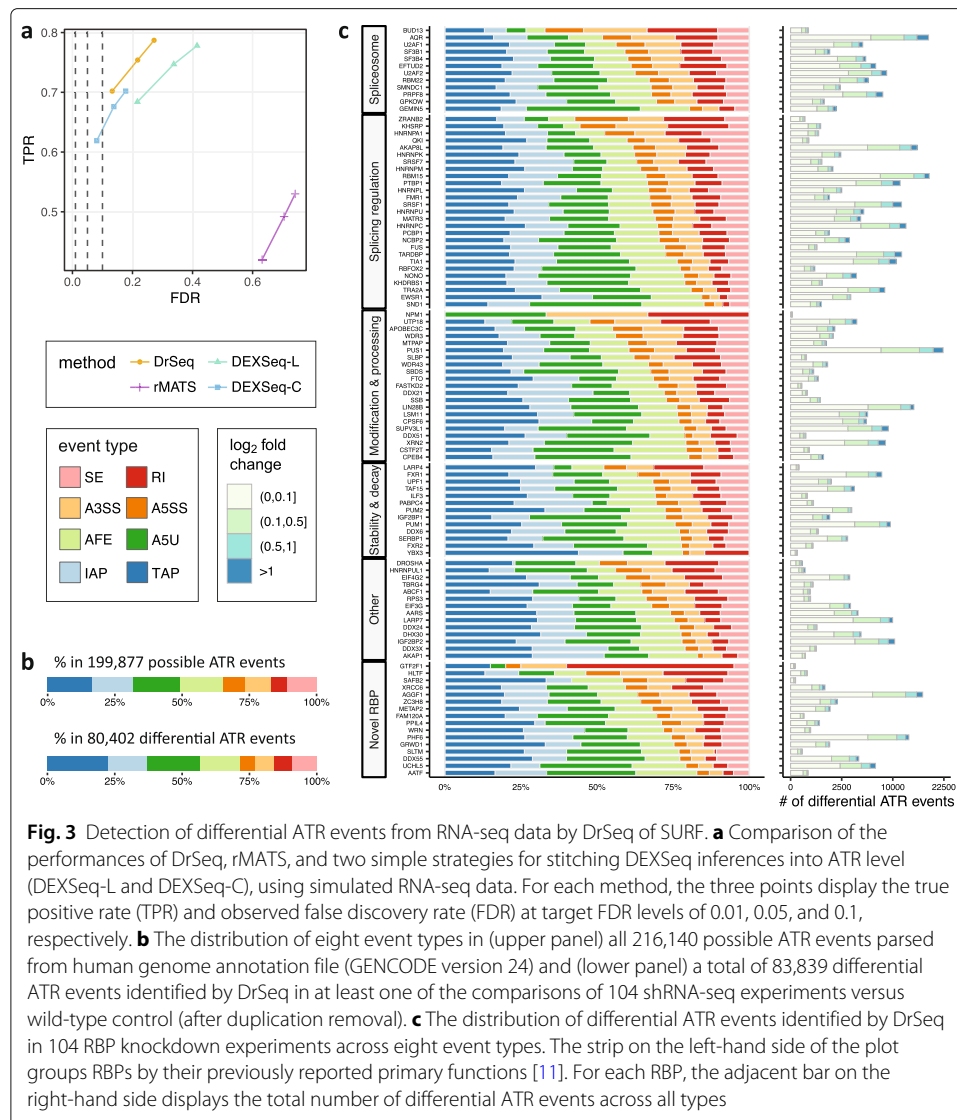


**Fig. 3** Detection of differential ATR events from RNA-seq data by DrSeq of SURF. **a** Comparison of the performances of DrSeq, rMATS, and two simple strategies for stitching DEXSeq inferences into ATR level (DEXSeq-L and DEXSeq-C), using simulated RNA-seq data. For each method, the three points display the true positive rate (TPR) and observed false discovery rate (FDR) at target FDR levels of 0.01, 0.05, and 0.1, respectively. **b** The distribution of eight event types in (upper panel) all 216,140 possible ATR events parsed from human genome annotation file (GENCODE version 24) and (lower panel) a total of 83,839 differential ATR events identified by DrSeq in at least one of the comparisons of 104 shRNA-seq experiments versus wild-type control (after duplication removal). **c** The distribution of differential ATR events identified by DrSeq in 104 RBP knockdown experiments across eight event types. The strip on the left-hand side of the plot groups RBPs by their previously reported primary functions [11]. For each RBP, the adjacent bar on the right-hand side displays the total number of differential ATR events across all types

difference between DrSeq and DEXSeq is mainly in their experimental units, which are ATR events and exonic bins, respectively.

Since a single ATR event typically spans multiple exonic bins, DrSeq combines data over exonic bins belonging to the same event and leads to better overall performance. In fact, the two “ad hoc” approaches we designed either have satisfactory FDR control at the expense of power loss or sustain a fairly large power while trading off FDR control. This analysis further supports that our extension of DEXSeq to ATR event level provides it with the competitive functionality as rMATS (i.e., event-level resolution) in addition to its unique feature of encompassing differential analysis of ATI and APA event classes.

### SURF reveals global positioning preferences of RBPs in AS, ATI, and APA events

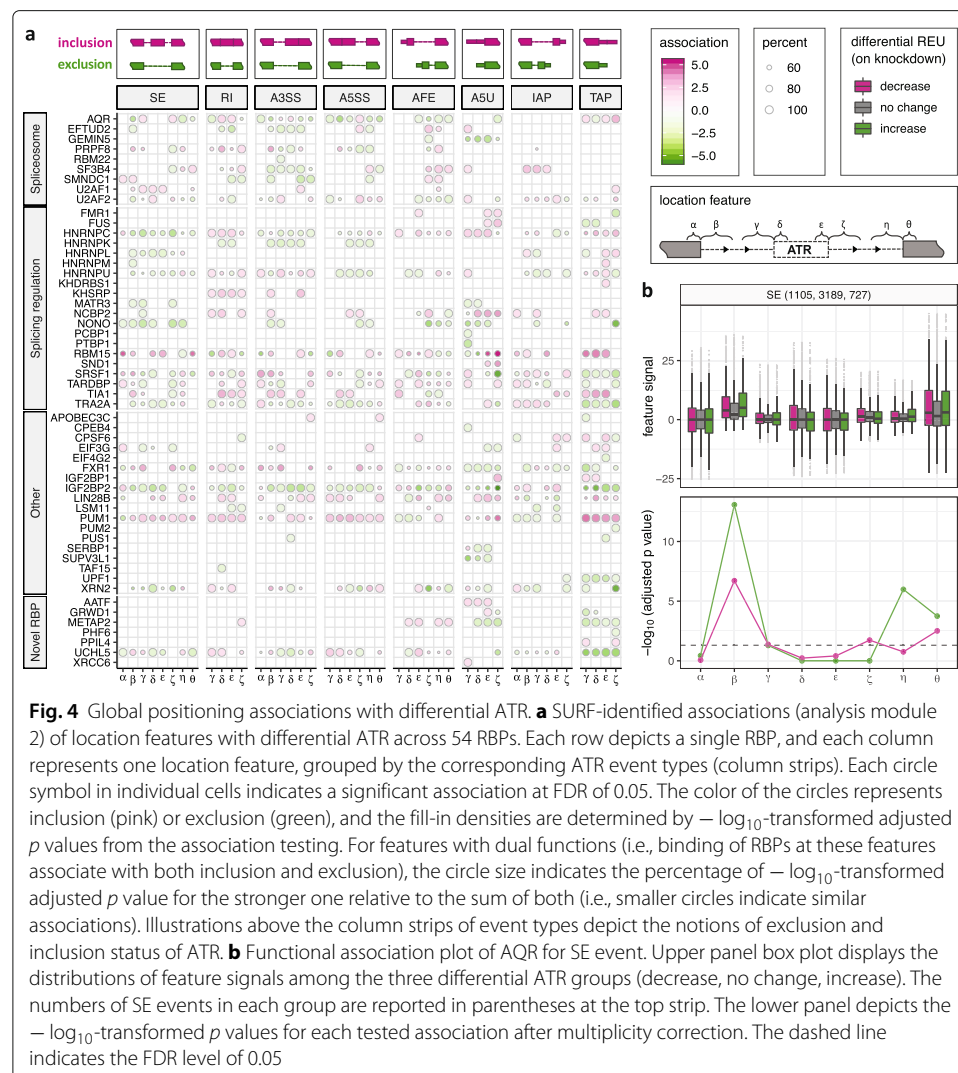
We applied SURF to a collection of 104 paired RNA-seq and eCLIP-seq datasets from the v78 release of the ENCODE project. We extracted AS, ATI, and APA events from a filtered version of the current human genome annotation file (GENCODE [36] version 24)

as described in the “[Materials and methods](#)” section. The filtering procedure was motivated by the observation that isoform pre-filtering improves performance of count-based methods for the analysis of differential transcript/exon usage [27] and resulted in 74,734 transcripts, 66,545 of which originated from protein coding genes. Collectively, these transcripts generated 199,877 AS, ATI, and APA events (upper panel in Fig. 3b). ATI and APA events constituted 65.31% of the total events with A5U at 17.50% and TAP at 16.86%, and SE, at 10.81%, was the most abundant category in AS.

Application of DrSeq to paired wild-type RNA-seq and shRNA-seq datasets of 104 RBPs in K562 cells identified 80,402 differential AS, ATI, and APA events (at FDR level of 0.05 and after duplication removal for analysis module 2). We observed that ATI and APA are the major sources of differential ATR (lower panel in Fig. 3b). In addition, we observed that a higher level of transcriptional complexity resulted from AS in the human genome than previously revealed by rMATS (Additional file 1: Fig. S13) [11]. Overall, these results reflect both the direct (i.e., through occupancy of events by RBPs) and indirect effects of RBPs on transcriptome and instigate the previously reported findings for *D. melanogaster* [37]. The observed complexity further accords with the results of a recent study on cross-tissue isoform differences [38]. Collectively, Fig. 3c shows the types and quantities of the differential ATR events. It highlights that (i) the impact of RBPs on ATR varies widely in magnitude (Fig. 3c); (ii) many RBPs affect a wide variety of ATR events (directly or indirectly), indicating a potentially complex co-regulating network of RBPs (e.g., AQR and SF3B4 as depicted by the volcano plots in Additional file 1: Figs. S14 and S15); and (iii) some RBPs exhibit event type specificity (e.g., CPSF6 exhibits evidence of TAP specificity, Additional file 1: Fig. S16).

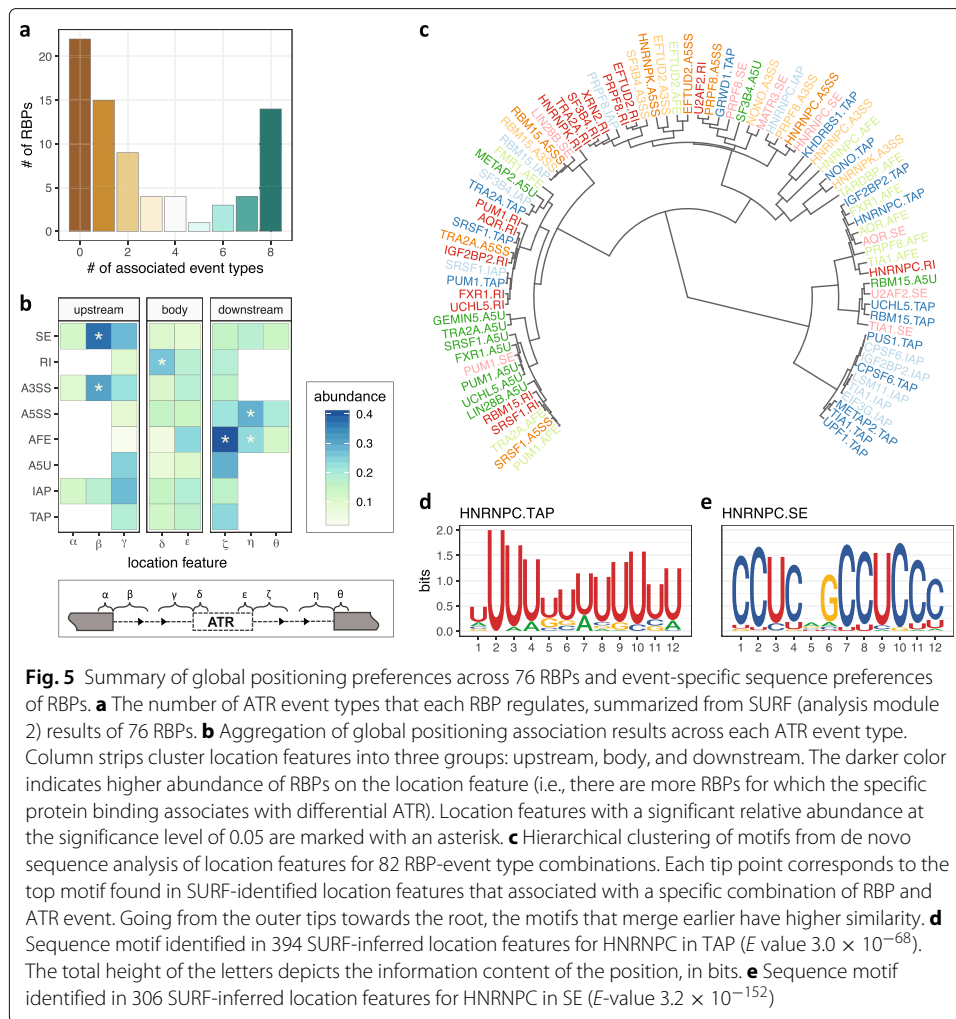
We next focused on 76 RBPs with eCLIP-seq data to study the direct effects of RBPs and their global positioning preferences for different types of ATR events. We limited our exposition to RBPs with at least 100 differential ATR events (i.e., increase or decrease upon knockdown) to enable association analysis. In addition, we estimated the average numbers of false positives in the association analysis by shuffling the grouping labels of differential ATR events and rerunning the analysis multiple times. This resulted in an average of 3.88 (with an s.d. of 2.38) false positive associations at target FDR level of 0.05 (Additional file 1: Table S3), indicating a conservative overall error control. Figure 4a reveals a large diversity in global positioning preferences for the 54 RBPs (see a full version of 76 RBPs in Additional file 1: Fig. S17) consistent with the earlier work [39]. Specifically, direct protein-RNA interactions of 14 RBPs significantly associate with differential ATR in all of the eight ATR event types, while some RBPs exhibit a more specialized association, e.g., 24 RBPs govern only one or two ATR event types (Fig. 5a). At the individual RBP level, SURF recapitulated known binding preferences for a number of spliceosome components [40], while revealing additional general trends of RBP interactions with RNA (Fig. 4a). Focusing on SE events, for instance, we observed that AQR and PRPF8 binding at the flanking intronic regions of event body (location features  $\gamma$  and  $\zeta$ ) associated with differential SE significantly (at FDR level of 0.05, Fig. 4b and Additional file 1: Figs. S18–S20). SF3B4 and SMNDC1 recognize the branching point (location feature  $\varepsilon$  of A3SS, Additional file 1: Fig. S5) of A3SS (Additional file 1: Figs. S21 and S22). In the class of ATI events, binding of GEMIN5 and AQR significantly associated with differential A5U (Additional file 1: Figs. S18 and S23), whereas U2AF1 and U2AF2 exhibited association with differential AFE (Additional file 1: Figs. S24 and S25). The latter further





suggested the involvement of spliceosomal components in recognizing alternative promoters [41]. In addition to these observations on spliceosomal components, SURF yielded various regulatory rules for non-spliceosomal RBPs. For example, we observed that CPSF6 [42] promotes the inclusion of the distal termination sites in regulating TAP (Additional file 1: Fig. S26), while UCHL5 promotes the exclusion of the distal termination sites in TAP (Additional file 1: Fig. S27).

While most global positioning tendencies of RBPs that associate with AS, ATI, and APA events (either previously reported [41, 43] or as revealed above) reside on or near the event body, our large-scale analysis with SURF instigates that many location features near the upstream (and sometimes downstream) constitutive exons of the ATR events also play fundamental roles in ATR through their interactions with RBPs. For example, SURF identified 21 RBPs as associating with SE by interacting at the intronic region adjacent to the upstream constitutive exon (location feature  $\beta$ ). We further assessed the overall significance of each feature by aggregating the SURF-identified global positioning associations across all the 76 RBPs for each individual event type (Fig. 5b) as described in the "Materials and methods" section. For SE events, the intronic region adjacent to upstream



constitutive exon ( $\beta$ ) exhibited marked enrichment compared to others with a  $p$  value of  $4.88 \times 10^{-4}$  according to Pearson's  $\chi^2$  test. The same observation held for A3SS events ( $p$  value of  $1.79 \times 10^{-4}$ , Pearson's  $\chi^2$  test) and highlighted the notable contribution from regions beyond proximal alternative splice sites. Overall, SURF identified 31 (40.7%) RBPs that showed evidence for interaction with features distal to the event body, suggesting a broader genomic scope of functional protein-RNA interactions than previously revealed.

#### SURF-identified location features carry ATR-specific sequence motifs

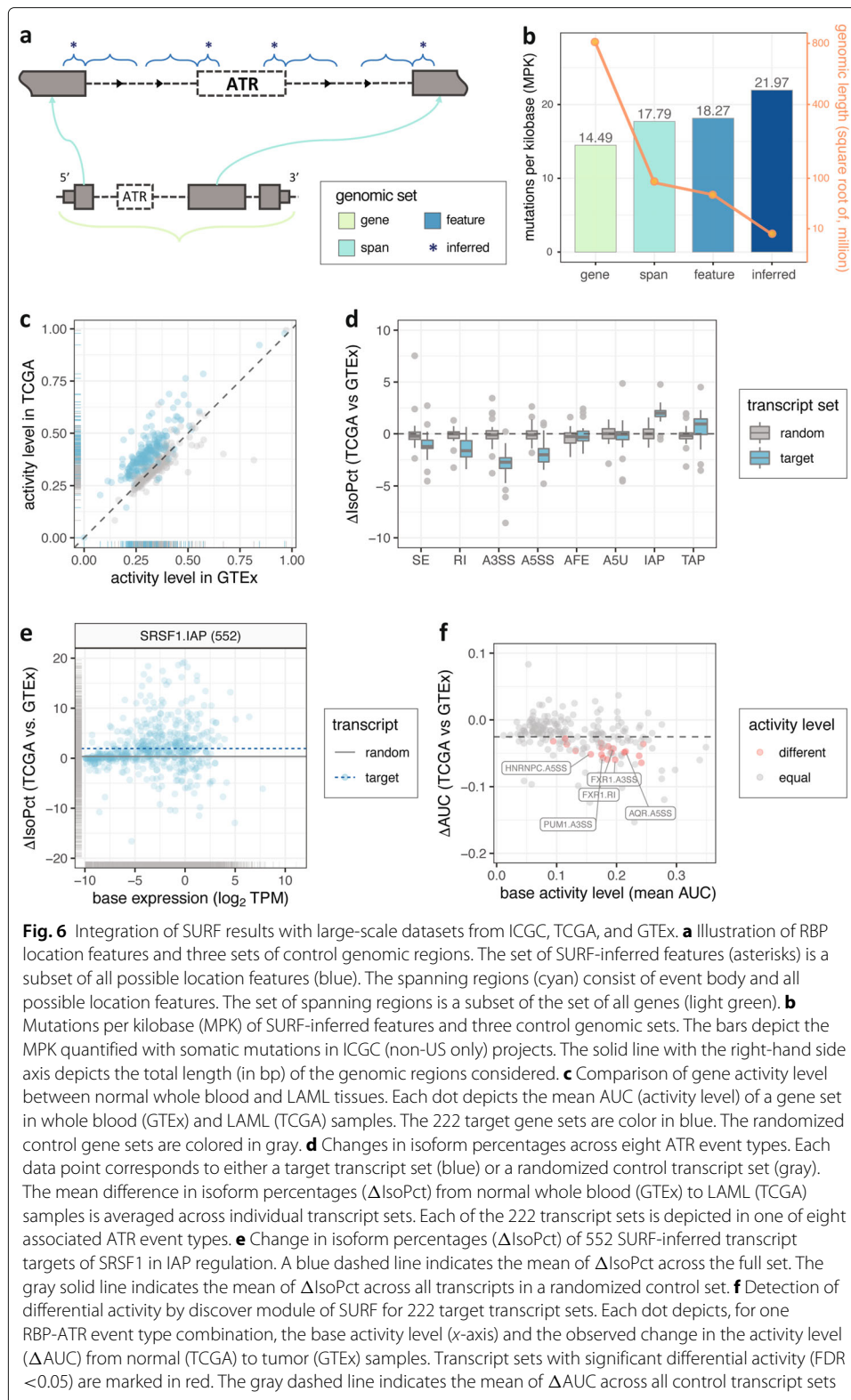
The analysis module 2 of SURF identified 34,795 differential ATR events associated with binding of at least one of 54 RBPs. Aggregation across these associations resulted in 71,667 SURF-inferred location features (at FDR level of 0.05 and feature signal cut-off of 20, the “Materials and methods” section), among which 34.9% (25,006) are associated with two or more RBPs. The numbers of inferred location features exhibited considerable heterogeneity across ATR types, with TAP having the largest numbers of inferred location features (19.2% and constituting 10.2% of all the possible location features of TAP event type), followed by A5U (15.5% and constituting 7.9% of all the possible location features of TAP event type) and SE (13.3% and constituting 5.5% of all the possible location features

of A5U event type) classes (Additional file 1: Fig. S28). Additional file 1: Fig. S29 displays the distribution of genomic coverage by inferred features for all the eight event types.

Recent machine learning applications to predict pre-mRNA processing highlighted strong predictive power of sequence variants [44–46]. While the SURF framework does not emphasize *in silico* prediction of ATR events from sequence input, we expected some location features to harbor sequence motifs for RBPs. Leveraging the ability of SURF to identify distinct location features for different ATRs regulated by the same RBP, we asked whether these location features harbored distinct sequence motifs. Specifically, we performed de novo motif analysis with the MEME suite [47] for location features of 222 RBP-ATR event type combinations involving 52 distinct RBPs (the “Materials and methods” section). This analysis captured a number of known, experimentally validated RBP motifs [48], e.g., TARDBP, U2AF2, HNRNPC, and TIA1. We next clustered these RBP-event type combinations, which involved 30 RBPs for which significant motifs were identified, based on the similarities of their identified motifs ( $E$  values  $\leq 0.01$ ) (Fig. 5c). The event type-based clustering evident in Fig. 5c is partly driven by the shared location features of RBPs for the same event type (Additional file 1: Fig. S30). However, the extent of overlap between the location features of different RBPs for the same event type is relatively low (Additional file 1: Fig. S31) and indicates marked contribution of sequence similarities of the RBP-event type-specific motifs to the clustering structure. Overall, de novo sequence analysis of SURF-inferred features unveiled multiple unique sequence motifs of RBPs for distinct ATR events. Specifically, 19 RBPs exhibited motif multi-modality of varying degrees which we quantified by the maximum and minimum Kullback-Leibler divergence between all the learnt PWMs of individual RBPs (Additional file 1: Fig. S32). For example, we observed that HNRNPC, a known poly(U)-binding regulator for the TAP class ( $E$  value  $3.0 \times 10^{-68}$ , Fig. 5d) [49–51], potentially recognizes a 5'-CCUC-3' motif for the SE class ( $E$  value  $3.2 \times 10^{-152}$ , Fig. 5e). Furthermore, this clustering reconfirmed that while TIA1 overall prefers uridine-rich sequences [52–54], it also interacts with an AU-riched sequences [55], 5'-AAUAAA-3', which resembles the canonical cleavage and polyadenylation site motif, in event types IAP and TAP in addition to two other significant motifs (Additional file 1: Fig. S33).

#### **SURF-identified location features are enriched for somatic mutations from ICGC and TCGA**

Recent studies highlighted central roles of RBPs in neurodegeneration, auto-immune defects, and cancer [56–64]. We hypothesized that the 71,667 location features associated with differential ATR events should harbor more somatic mutations than expected by chance or expected in comparable regions of the genome not necessarily associated with such ATR events. To test this, we leveraged genome-wide mutation data from ICGC (excluding US projects as they only contained coding mutations) and coding mutations from TCGA. Noting that the set of SURF-inferred features is a subset of all possible location features extracted from genome annotation, we designed the following control sets: (i) the full set of location features, (ii) union of span of events where the span is defined as the event body and its location features, (iii) genomic span of genes harboring all the events with an extension by 300 bp upstream of transcription start sites and downstream of transcription end sites. These control sets form a nested set of regions from (i) to (iii) (Fig. 6a). Then, we calculated mutation per kilobase (MPK) as a measure of mutation quantification for each set of the genomic sets (Fig. 6b and Additional



file 1: Fig. S34). We observed an increasing enrichment of somatic mutations from genes to SURF-inferred features ( $p$  value  $3.00 \times 10^{-4}$  from an exact Poisson test with a fold change of 1.50, Additional file 1: Table S4). This enrichment highlights that location fea-

tures inferred as associated with differential ATR events by SURF harbor markedly more somatic mutations compared to a large class of control sets. In addition, SURF-inferred location features also harbored more somatic mutations than the regions significantly bound in eCLIP-seq data (i.e., peaks with IDR <0.01, covering a total length of 30.77 million bp and with an MPK of 17.08 compared to the 21.97 MPK of SURF-inferred location features,  $p$  value  $5.138 \times 10^{-5}$  from an exact Poisson test with a fold change of 1.27). A similar result continued to hold with TCGA mutation data and is available from Additional file 1: Fig. S35 and Table S5.

### **SURF-identified ATR targets of RBPs exhibit differential transcriptional activity between TCGA acute myeloid leukemia tumor and GTEx whole blood samples**

We next performed a comparative analysis of transcriptional activity of genes and transcripts harboring specific RBP-ATR event type combinations in normal versus tumor samples by leveraging GTEx and TCGA resources. We specifically considered TCGA LAML sample for which the K562 erythroleukemic cell line has the most relevance for. Harnessing of gene and transcript targets based on SURF-inferred location features capitalizes our construction of location features—each location feature is designated to a single ATR event that originates from a unique transcript. Among the 222 available RBP-ATR event type combinations, 132 (or 131) of them had more than 100 genes (or transcripts) with at least one SURF-inferred location feature (Additional file 1: Fig. S36). On average, protein-coding genes compromised 97.3% of all the gene sets. We first asked whether the activity of an RBP, as measured by expression of its target genes, significantly varied between 173 GTEx whole blood samples and 337 TCGA LAML samples (Additional file 1: Fig. S37). To account for potential within cohort biases of the RNA-seq data, we constructed randomized control sets for each gene set by matching their sizes and average activity levels (as measured by AUC, the “Materials and methods” section). With such control, we observed a general shift of target gene activity from normal to tumor tissues (Fig. 6c and Additional file 1: Fig. S38), suggesting potential importance of SURF-identified RBP targets for LAML.

We next queried whether specific transcript targets of RBPs behaved differentially among all isoforms originating from the same gene, across tissue conditions. To this end, for every transcript, we quantified the changes in isoform percentage ( $ISO_{Pct}$  as reported by RSEM) from GTEx whole blood samples to TCGA LAML samples. Isoform percentage of a transcript depicts the percentage of its abundance over its parent gene's abundance, and its comparison across conditions elucidates how the contribution of a transcript to overall gene abundance is changing across conditions. Comparison of isoform percentages revealed a diverse pattern across ATR event types (Fig. 6d), suggesting a refined transcript-level biological relevance of SURF-identified RBP targets. Specifically, the transcript sets associated with AS events (AS, RI, A3SS, and A5SS) exhibited reduced isoform percentage (as compared to matched random control sets from other isoforms originating from the same gene) between normal (GTEx) and tumor (TCGA) tissues (Additional file 1: Fig. S39). In contrast, the transcript sets associated with APA events (namely IAP and TAP) exhibited increased isoform percentage in tumor samples compared to normal samples (e.g., SRSF1 in IAP, Fig. 6e), indicating that the transcripts harboring these event types contributed more to their parent gene's overall abundance. This observation is further supported by multiple replicates of random control and after

de-duplicating transcripts across event types (Additional file 1: Figs. S40 and S41). Since ATR events are defined by variable bins, which originate from shorter transcripts (i.e., those with absent exonic parts), this observation suggests that the transcripts that terminate earlier at 3' end, as well as those with more internal "spliced-in" exonic parts, tend to be more transcriptionally active in the LAML cancer tissues compared to normal blood tissues. Shortening of 3' UTRs is widely observed during tumorigenesis and cancer progression [65, 66]. In addition to supporting this widely observed phenomenon, our results suggest that AS and APA events contribute more to transcriptome diversity in cancer compared to ATI events.

To test the differential activity for individual transcript sets, we applied the discovery module of SURE, with their paired controls by including the transcripts originating from the same corresponding target genes. Of all the RBP-ATR event type combinations, 18 of them (among the 131 with more than 100 transcripts) exhibited significantly different transcriptional activity between the whole blood (GTEx) samples and LAML (TCGA) samples, at FDR cut-off of 0.05 (Fig. 6f). The detected transcript sets originate from 9 RBPs, among which FXR1, SRSF1, and U2AF2 associate with the most diverse ATR event types (SE, A3SS, A5SS for all three RBPs, and RI for FXR1 additionally), followed by AQR and HNRNPC through two event types (Additional file 1: Table S6), many of which have previously reported implications in cancer (e.g., [67, 68]). All but two of these RBPs (FXR1 and PUM1) are splicing factor genes and U2AF1 exhibited significant driver mutation patterns across a wide variety of cancer types [63].

## Discussion and conclusions

In this study, we presented SURE, a new integrative framework for the analysis of large-scale CLIP-seq and coupled RNA-seq data and applied it to ENCODE consortium data (Table 1). A key advancement in SURF is the extension of differential exon usage method DEXSeq to differential alternative transcriptional regulation at the event level. We presented a formulation, DrSeq, that avoided ad hoc downstream analysis stitching DEXSeq results into event level, while controlling FDR and achieving as well or better power than alternatives. In addition, DrSeq uniquely enabled differential ATR detection for alternative transcription initiation and alternative polyadenylation events, a feature currently lacking in the widely adapted tool rMATS. SURF performs all integrated analyses based on the AS, ATI, and APA events as experimental units. Event-centric analyses are preferred when focusing on alternative splicing at the level of individual splicing events, e.g., the inclusion of a skipped exon, or the usage of a particular alternative splicing site. Interpreting the results of event-centric analyses is straightforward, and follow-up validation experiments for differential AS, ATI, and APA events are easier to design.

**Table 1** Overview of the data used by individual modules of SURF

Module	No. of RBPs	Input datasets (sources)
1 – DrSeq	104	104 shRNA-seq with paired control RNA-seq from wild-type condition (ENCODE)
2 – Association	76*	76 eCLIP-seq with paired control datasets from size-matched input library (ENCODE)
3 – Discovery	54**	173 whole blood RNA-seq (GTEx) and 337 LAML RNA-seq (TCGA)

\*RBPs lacking at least 100 differential ATR events are excluded from the analysis module 2

\*\*The discovery module studies a subset of RBPs in \* with at least one inferred location feature

Association of DrSeq-identified differential ATR results to global positioning preferences of RBPs with eCLIP-seq data revealed large diversity among RBPs and suggested dual inclusion and exclusion roles for RBPs based on the positioning of protein-RNA interactions. Furthermore, aggregation of the positioning preferences across RBPs within each event type revealed that locations near the upstream and sometimes downstream constitutive exons of the ATR events also play a significant role in ATR. Sequence analysis of SURF-inferred location features (e.g., regions that SURF deemed as significantly related to ATR) revealed known and novel interaction modalities for RBPs in ATR. To further assess the overall relevance and importance of SURF-inferred location features, we compared the somatic mutation densities of these regions with carefully designed controls. This analysis revealed that location features inferred as associated with differential ATR events harbored significantly more somatic mutations both in ICGC and TCGA consortia data. Further integration with reference transcriptomes from GTEx and TCGA highlighted contribution of APA and AS regulation in diverse transcriptome activity in cancer and revealed RBPs with ATR event-specific differential transcriptional activities in LAML tumors compared to GTEx normals.

SURF presents the first framework for systematic integrative analysis of large collections of CLIP-seq and RNA-seq data and includes a discovery module for probing public TCGA and GTEx transcriptome data. This comprehensive approach coupled with the ability to identify differential ATR events from settings with multiple biological replicates underlines SURF's potential as an integrative tool. There are a number of directions that naturally build on the results of SURF. Since we have observed significant enrichment of somatic mutations from ICGC and TCGA in SURF-identified location features, evaluation of impact of individual somatic mutations on RBP binding with *in silico* calculations [69, 70] could elucidate how such mutations might be manifesting their effects. SURF focused on each RBP marginally. Given the complex combinatorial nature of ATR [11, 43], a promising extension to SURF framework should be in the direction of multivariate analysis of large collections of RBPs.

## Materials and methods

### Isoform pre-filtering

In order to improve FDR control, we pre-filtered transcripts in the human genome annotation file (GENCODE version 24) before extracting ATR events, as suggested by [27]. We performed the filtering based on the RSEM [71] transcriptome quantification of 486 RNA-seq datasets, including 220 RBP knockdown experiments (with two replicates) and 23 wild-type control experiments (with two replicates). Specifically, the transcripts with (i) relative isoform abundance estimate ( $\text{IsoPct}$ , IP) of less than  $c\%$  across all samples or (ii) TPM estimate less than 1 across all samples were removed. We varied the threshold  $c$  for filtering relative isoform abundance as 5%, 10%, and 25% and considered the following strategies: (1)  $\text{IP} \geq 5\%$ , (2)  $\text{IP} \geq 10\%$ , (3)  $\text{IP} \geq 25\%$ , (4)  $\text{TPM} \geq 1$ , and (5)  $\text{IP} \geq 5\%$  and  $\text{TPM} \geq 1$ . Additional file 1: Table S7 summarizes the filtering thresholds, the number of retained genes, transcripts, and the sum of TPM (averaged across all samples). The total read counts aggregated across transcripts appeared similar to the sum of TPM, thus are omitted from the table. This investigation suggested that isoform pre-filtering markedly reduces the transcriptome complexity of the raw genome annotation, while possessing the vast majority of transcriptome signals. In fact, 70% of the genes in the filtered set were

protein-coding as opposed to 32% in the original file. This implies that majority of the filtered transcripts are from non-coding genes.

#### **Parsing AS, ATI, and APA events from genome annotation**

The parsing procedure consists of two steps. First, we define *variable* bins of exonic regions for each transcript as the set of absent exonic regions of the transcript compared to the full gene model (Additional file 1: Fig. S3). This definition is previously introduced by [33], and it enjoys the property that all variable bins of a transcript are mutually disjoint. We group runs of variable bins (i.e., merge any consecutive ones within the transcript) and categorize each as an ATR *event*. In the second step, we invoke a decision tree to uniquely annotate each event to a specific category among alternative splicing (AS) events including exon skipping (SE), alternative 3' (A3SS) or 5' (A5SS) splicing, intron retention (RI), alternative first exon (AFE), alternative 5'UTR (A5U), and intronic (IAP) or tandem (TAP) alternative polyadenylation, according to its relative position within the gene (Additional file 1: Fig. S4). Note that all the ATR events from one transcript are isolated from each other, which essentially forges the uniqueness of event annotations. Finally, we deduplicated the events from different transcripts of the same gene that (i) shared the same genomic information (coordinates, strand, and constitutive upstream/downstream exons) and (ii) were classified into the same event type.

#### **Extracting location-specific features**

We generated a set of location features relevant to the ATR events according to their event types (Additional file 1: Fig. S5). These location features were designed to capture RBP binding signals in the upstream/downstream constitutive exons of the event, starting and end sites of the event body, as well as adjacent intronic regions. For example, an SE event has eight location features: two 100-bp regions from the upstream and downstream constitutive exons, four 300-bp regions from two flanking introns (upstream and downstream) of the event body (i.e., the cassette exon), and two 100-bp flanking regions spanning the start and end of the event body (Fig. 2c). For the flanking or spanning regions that were shorter than the desired length of 100 bp or 300 bp, we used one half of the exonic or intronic length. The number of location features for the other ATR event types ranges between 4 and 8. Each location feature represents a global positioning preference that potentially associates with the DrSeq-inferred differential ATR status. Detailed pictorial illustrations of location features for each event type are depicted in Additional file 1: Fig. S5.

#### **DrSeq for detecting differential alternative transcriptional regulation**

Differential ATR event detection is performed in two phases: RNA-seq read counting and statistical inference. The entire procedure takes as input the annotation of ATR events and the aligned reads from RNA-seq samples and outputs for each ATR event the result of differential testing including the test statistics, *p* values, estimated log<sub>2</sub> fold changes, and additional summary objects. For each event, DrSeq counts RNA-seq reads at two levels, event body and the gene to which the event belongs, by resorting to `featureCounts` [72]. While this counting scheme allows reads to overlap multiple events or genes, diagnostic plots did not reveal any adverse effects (Additional file 1: Fig. S42). Since DrSeq tests for each event separately, each read is used at most once in each test. DrSeq



invokes DEXSeq as an inference engine to fit the differential ATR model (1). Specifically, the events are grouped by their types and model fitting is performed separately. This allows capturing the mean-dispersion relationships in an event type-specific manner and reduces dependency among the tests (Additional file 1: Fig. S43). After the model fitting and testing, all  $p$  values are jointly corrected for multiplicity with the BH procedure.

#### Simulation design for differential ATR detection

We simulated RNA-seq data following the strategy by [27]. First, RSEM model parameters were estimated from two real RNA-seq assays (ArrayExpress dataset E-MTAB-3766 in [73]). Then, a mean/dispersion relationship, learnt from real data [74], was used to generate samplewise transcript expression estimates, for three replicates of the wild-type and three replicates of differential conditions. To create the differential condition, we sampled 1000 genes and introduced differential transcript usage by switching the relative abundances for the two most expressed transcripts. These genes were selected randomly among those with sufficiently high expression (expected count greater than 500) and at least two sufficiently highly expressed isoforms (i.e., with relative expression abundance, as calculated by RSEM, above 10%). Since the isoforms have varying lengths, the expected read count for these genes varied between the conditions, while the TPM remained similar. This procedure generated a spectrum of differential ATR events and eliminated potential confounding due to gene-level differential expression. Finally, we used RSEM to simulate paired fastq files with a read length of 101 bp for each sample. For DrSeq, we used the default pipeline. For DEXSeq, we used default settings with the exception of invoking the `-r no` configuration to avoid merging overlapping genes into complexes. For rMATS (version 4.0.2), we used the default cut-off of 0.0001 for splicing difference and employed the same FDR thresholds as DrSeq. For MAJIQ (version 2.1), we administered both the default setting and a liberal setting where the change threshold of MAJIQ (`-threshold`) was set to 0.1.

#### Read coverage of ATR events from RNA-seq

In the analysis module 2 of SURE, we filtered out (i) low coverage events and (ii) overlapping ATR events of the same type to avoid near-duplication observations in the association analysis. Specifically, we employed a *read coverage* measure that is akin to the Fragments Per Kilobase Million (FPKM) in transcriptome quantification for RNA-seq. For a given event, we first counted the number of reads residing on the event body (in million), where we utilized only the reads with mapping quality score greater than 10 (this threshold also applies to eCLIP-seq reads). To account for sequencing depth differences, the counts were then normalized by the size factor of each sample [75] and averaged across all four samples (two replicates per condition). We refer the resulting quantity as the *base mean*, which is also reported by DrSeq. Next, we adjusted the base mean by dividing it with the pseudo length of each event (in kilobase) and used this adjusted mean as the coverage of ATR events. Here, the *pseudo length* of an ATR event is defined as its actual length (in kilobase) shifted by the read length minus one, that is, 99 bp (all shRNA-seq experiments from the ENCODE consortium have the same read length of 100 bp). The adjustment with pseudo length (as opposed to the actual length) regularized those extremely short (in length) ATR events and reduced the effects of overlapping counting. This had negligible effect on long ATR events. Finally, we excluded any ATR events with

read coverage smaller than 0.05, and among the overlapping ATR events, we only kept the event with the highest read coverage for the downstream analysis.

#### Generation of feature signals from eCLIP-seq data

Each ATR event has a set of location features, each of which is a genomic region of potential protein-RNA interaction. This step of SURF takes as input the aligned reads from the IP and accompanying control input samples of eCLIP-seq and summarizes the eCLIP-seq signals at these features. To this end, for each feature, it first counts the number of overlapping reads (in million) in each sample by requiring an overlap of at least 12 bp between the read and the location feature. The 12 bp corresponds to the 25% of the read length in the ENCODE eCLIP-seq experiments. Then, the read counts are normalized by the sequencing depth of each sample. Next, the normalized read counts are weighted by the genomic length (in kilobase) of the feature, which is then averaged separately across the IP and control input samples. Finally, the difference between normalized IP and input samples is reported as *feature signal*.

#### Association analysis for global positioning preferences

We used a logistic regression framework to derive global positioning preferences, e.g., position-specific rules for RBPs in regulating ATR. Specifically, for each event  $i$  with event type  $\tau(i) = t$ , let  $x_{ik}$  denote the feature signal at the  $k$ th location feature. The random variable  $Y_i \sim \text{Bernoulli}(p_t)$  corresponds to whether an event is differentially regulated ( $Y_i = 1$ ) or not ( $Y_i = 0$ ). We link its mean parameter  $p_t$  to the eCLIP-signals of the location features marginally with a logit function as

$$\log\left(\frac{p_t}{1-p_t}\right) = \beta_t^A + \beta_{ik}^F x_{ik}. \quad (2)$$

Here, parameter  $\beta_t^A$  represents the grand effect of ATR event  $t$  and quantifies a baseline for the probability of observing a differential ATR event. This parameter also accounts for the position independent effects of RBP in regulating this event type. Position-specific main effect  $\beta_{ik}^F$  captures the global positioning effect of RBP at the specific location feature  $k$ .

In fitting the above model for every ATR event type  $t$ , we also considered increased and decreased regulation separately: model for  $Y_i = 1$  corresponds to increased regulation ( $p$  value  $< 0.05$  and  $\log_2$  fold change  $> 0$ ) and model for  $Y_i = 0$  represents decreased regulation ( $p$  value  $< 0.05$  and  $\log_2$  fold change  $< 0$ ). Both models incorporated the same set of equal regulation (i.e., “no change”) events for  $Y_i = 0$  ( $p$  value  $> 0.4$ ). The reason for separating increased and decreased regulation is primarily due to the possibility that interactions of a single RBP at a specific pre-mRNA location feature might result in both inclusion and exclusion of the alternative site, depending on the presence/absence of other collaborative/competitive RBPs. Differential ATR analysis of the ENCODE compendium data of 104 RBPs with module 1 of SURF resulted in, on average and after filtering out overlaps, 2182.02 (1.01% of all tested events) events with increased REU and 1914.98 (0.89% of all tested events) events with decreased REU. This enabled fitting of model (2) and testing of the position-specific main effect parameter  $\beta_{ik}^F$  by a standard likelihood

ratio test. Tests for all the location features were corrected for multiplicity with the BH procedure at FDR level of 0.05.

#### Summarizing association tests across RBPs

We quantified the abundance of a location feature by the normalized number of RBPs that significantly associated with it. Specifically, we aggregated the results of global positioning associations across all the 76 RBPs for each individual event type. For each RBP and each event type, we first applied minus logarithm (base 10) transformation on  $p$  values and normalized them to have unit sum. The normalization accounts for the fact that an RBP may interact with its target RNA (pre-mRNA) at multiple location features. Then, for every event type, these values were averaged across RBPs and interpreted as *feature abundance* (Fig. 5c). Next, we evaluated whether any of the features were significantly more abundant in comparison to other features of the same ATR event type by Pearson's  $\chi^2$  test on two variables denoting (i) whether or not a location feature is significantly associated with the differential ATR and (ii) whether or not the location feature is  $x$ , where  $x \in \{\alpha, \beta, \dots, \theta\}$  is the location feature for that ATR event type. All the tests employed Yates's correction for continuity.

#### Extracting SURF-inferred location features

As a result of association testing in the analysis module 2 of SURE, each location feature is assigned a  $p$  value (adjusted for multiplicity when appropriate). SURF then generates a list of *inferred* location features by filtering as follows. First, it selects statistically significant location features at FDR of 0.05. Note that each selected feature has a corresponding training dataset, which consists of differential ATR events and control events. SURF then extracts the list of genomic regions for each selected location feature from this corresponding set of differential ATR events. Finally, leveraging the quantified feature signals from the analysis module 2, it filters out the genomic regions with feature signals, i.e., normalized background adjusted eCLIP-seq read counts, below 20 and defines the set of remaining genomic regions as the inferred features. Imposing the eCLIP-seq signal condition ensures that the set reflects the consequences of *direct* protein-RNA interaction. Note that the inferred features are event-specific and are associated with specific regulation status. As a result, each inferred feature has its associated ATR event and inferred RBP regulation function (i.e., "inclusion" or "exclusion").

#### Sequence analysis for SURF-inferred location features

For SURF-inferred features, we performed de novo motif discovery using the MEME-suite [76], with a zero or one occurrence per sequence (ZOOPS) model in the default mode with background distribution estimated from the input sequences. Specifically, we extracted the genome sequence (human genome version GRCh38) of each SURF-inferred location features, which were then assembled into 326 various collections based on their associated ATR event type, RBP, and feature type (e.g.,  $\alpha, \beta, \dots$ ). The collections of interest corresponded to (i) 52 individual RBPs, (ii) 8 types of ATR events, (iii) 44 event  $\times$  location feature combinations (e.g., SE- $\alpha$ , SE- $\beta$ , etc.), and (iv) 222 RBP-ATR event type combinations (e.g., SRSF1-SE). Finally, we searched for the top 3 motifs with the minimum width of 5 bp and the maximum of 12 bp in each collection of sequences, where we filtered the resulting motifs by minimum occurrences of 40 times. The SURF-inferred location

features and the output of 326 individual MEME runs (version 5.0.5) are deposited (see Availability of supporting data). For clustering of identified motifs, we used a metric based on Kullback-Leibler divergence of position weight matrices (PWMs) as adapted in [77] and Wald's agglomeration method [78].

### Differential activity of transcript sets

The discovery module of SURF takes in sets of RBP targets (e.g., transcripts or genes that harbor SURF-inferred location features) and perform differential analysis on these sets across conditions, in terms of their activity. This module adapts a rank-based approach, inspired by the single-cell RNA-seq application of [35], to score the *activity* of a target set in a sample by the AUC. The AUC evaluates the ranking of its elements compared to other quantified units in the sample in terms of expression (Additional file 1: Fig. S6). As a result, it transforms the transcriptome expression across samples into a measure of activity across samples and enables testing of differential activity across conditions. To calibrate the activity scores within each condition, this module also allows a paired control set for each target set. To enable subsampling for generating a null distribution, the control set is preferably larger in size than the corresponding target set. The differential analysis then tests for the difference in AUC between the two conditions using the difference in AUC. Our test statistic is the difference in AUC between the two conditions (e.g., GTEx vs. TCGA). An empirical null distribution for this statistic is estimated by randomly subsampling from the control set 5000 times. Each subsampling matches the size of the target set. The  $p$  values are adjusted to control for FDR using the BH procedure (see Additional file 1: Fig. S44 for the histogram of raw  $p$  values realized with 222 target transcript sets).

### Supplementary information

**Supplementary information** accompanies this paper at <https://doi.org/10.1186/s13059-020-02039-7>.

**Additional file 1:** Supplementary Figs. S1-S44 and Tables S1-S7.

**Additional file 2:** Review history.

### Peer review information

Andrew Cosgrove was the primary editor of this article and managed its editorial process and peer review in collaboration with the rest of the editorial team.

### Acknowledgements

We are grateful to Michael Cammilleri for his endless technical support in high-throughput computing. We thank Marvin Wickens, Judith Kimble, Heidi Dvinge, Brian Carrick, and members of Keleş Group for many helpful discussions. We also thank the anonymous reviewers for their detailed comments that led to improvements in the manuscript.

### Review history

The review history is available as Additional file 2.

### Authors' contributions

SK conceived and supervised the project. SK and FC designed the research and developed the methods. FC implemented and carried out the experiments. SK and FC interpreted the results. SK and FC wrote the paper. Both authors read and approved the final manuscript.

### Authors' information

Twitter handle: @fchen365 (Fan Chen).

### Funding

This work was supported by National Institutes of Health grants HG007019, HG003747, and U54AI117924 and the Center for Predictive Computational Phenotyping (CPCP) grant (SK).

**Availability of data and materials**

The datasets supporting the conclusions of this article are available in the following repositories. The human genome annotation file (version 24) is available from the GENCODE project [36], <https://www.genencodegenes.org>. The shRNA-seq and the eCLIP-seq datasets were accessed from the ENCODE project [9], <https://www.encodeproject.org>, lastly on October 28, 2018. The somatic mutation datasets for both the TCGA and ICGC projects and the transcript expression datasets (RSEM quantification) for both the TCGA and the GTEx projects were downloaded from the UCSC Xena platform [79], <http://xena.ucsc.edu>. The processed data and the results of SURF analysis are deposited at Zenodo, <https://doi.org/10.5281/zenodo.3779037> [80]. The source code for reproducing the results of this paper is released at GitHub under the GPL 3.0 license, <https://github.com/keleslab/surf-paper> [81].

**Ethics approval and consent to participate**

Not applicable

**Consent for publication**

Not applicable.

**Competing interests**

The authors declare that they have no competing interests.

Received: 2 December 2019 Accepted: 8 May 2020

Published online: 12 June 2020

**References**

- Wang ET, Sandberg R, Luo S, Khrebtkova I, Zhang L, Mayr C, et al. Alternative isoform regulation in human tissue transcriptomes. *Nature*. 2008;456(7221):470.
- Kalsotra A, Cooper TA. Functional consequences of developmentally regulated alternative splicing. *Nat Rev Genet*. 2011;12(10):715.
- Nilsen TW, Graveley BR. Expansion of the eukaryotic proteome by alternative splicing. *Nature*. 2010;463(7280):457.
- Franks A, Airolidi E, Slavov N. Post-transcriptional regulation across human tissues. *PLoS Comput Biol*. 2017;13(5):e1005535.
- Licatalosi DD, Mele A, Fak JJ, Ule J, Kayikci M, Chi SW, et al. HITS-CLIP yields genome-wide insights into brain alternative RNA processing. *Nature*. 2008;456(7221):464.
- Khalil AM, Guttman M, Huarte M, Garber M, Raj A, Morales DR, et al. Many human large intergenic noncoding RNAs associate with chromatin-modifying complexes and affect gene expression. *Proc Natl Acad Sci*. 2009;106(28):11667–72.
- Van Nostrand EL, Pratt GA, Shishkin AA, Gelboin-Burkhart C, Fang MY, Sundararaman B, et al. Robust transcriptome-wide discovery of RNA-binding protein binding sites with enhanced CLIP (eCLIP). *Nat Methods*. 2016;13(6):508.
- de Klerk E, ACt Hoen P. Alternative mRNA transcription, processing, and translation: insights from RNA sequencing. *Trends Genet*. 2015;31(3):128–39.
- Consortium EP, et al. The ENCODE (ENCyclopedia of DNA elements) project. *Science*. 2004;306(5696):636–40.
- Consortium EP, et al. Identification and analysis of functional elements in 1% of the human genome by the ENCODE pilot project. *Nature*. 2007;447(7146):799.
- Van Nostrand EL, Freese P, Pratt GA, Wang X, Wei X, Blue SM, et al. A large-scale binding and functional map of human RNA binding proteins. *bioRxiv*. 2018179648.
- Yee BA, Pratt GA, Graveley BR, Van Nostrand EL, Yeo GW. RBP-Maps enables robust generation of splicing regulatory maps. *RNA*. 2019;25(2):193–204.
- Lonsdale J, Thomas J, Salvatore M, Phillips R, Lo E, Shad S, et al. The genotype-tissue expression (GTEx) project. *Nat Genet*. 2013;45(6):580.
- Tomczak K, Czerwińska P, Wiznerowicz M. The Cancer Genome Atlas (TCGA): an immeasurable source of knowledge. *Contemp Oncol*. 2015;19(1A):A68.
- Katz Y, Wang ET, Airolidi EM, Burge CB. Analysis and design of RNA sequencing experiments for identifying isoform regulation. *Nat Methods*. 2010;7(12):1009.
- Shen S, Park JW, Huang J, Dittmar KA, Lu ZX, Zhou Q, et al. MATS: a Bayesian framework for flexible detection of differential alternative splicing from RNA-seq data. *Nucleic Acids Res*. 2012;40(8):e61.
- Wang W, Qin Z, Feng Z, Wang X, Zhang X. Identifying differentially spliced genes from two groups of RNA-seq samples. *Gene*. 2013;518(1):164–70.
- Norton SS, Vaquero-Garcia J, Lahens NF, Grant GR, Barash Y. Outlier detection for improved differential splicing quantification from RNA-seq experiments with replicates. *Bioinformatics*. 2018;34(9):1488–97.
- Shen S, Park JW, Lu ZX, Lin L, Henry MD, Wu YN, et al. rMATS: robust and flexible detection of differential alternative splicing from replicate RNA-seq data. *Proc Natl Acad Sci*. 2014;111(51):E5593–601.
- Tian B, Hu J, Zhang H, Lutz CS. A large-scale analysis of mRNA polyadenylation of human and mouse genes. *Nucleic Acids Res*. 2005;33(1):201–12.
- Shepard PJ, Choi EA, Lu J, Flanagan LA, Hertel KJ, Shi Y. Complex and dynamic landscape of RNA polyadenylation revealed by PAS-Seq. *RNA*. 2011;17(4):761–72.
- Ha KC, Blencowe BJ, Morris Q. QAPA: a new method for the systematic analysis of alternative polyadenylation from RNA-seq data. *Genome Biol*. 2018;19(1):45.
- Trapnell C, Roberts A, Goff L, Pertea G, Kim D, Kelley DR, et al. Differential gene and transcript expression analysis of RNA-seq experiments with TopHat and Cufflinks. *Nat Protocol*. 2012;7(3):562.
- Hu Y, Huang Y, Du Y, Orellana CF, Singh D, Johnson AR, et al. DiffSplice: the genome-wide detection of differential splicing events with RNA-seq. *Nucleic Acids Res*. 2012;41(2):e39.

25. Aschoff M, Hotz-Wagenblatt A, Glatting KH, Fischer M, Eils R, König R. SplicingCompass: differential splicing detection using RNA-seq data. *Bioinformatics*. 2013;29(9):1141–8.
26. Shi Y, Jiang H. rSeqDiff: detecting differential isoform expression from RNA-Seq data using hierarchical likelihood ratio test. *PLoS One*. 2013;8(11):e79448.
27. Soneson C, Matthes KL, Nowicka M, Law CW, Robinson MD. Isoform prefiltering improves performance of count-based methods for analysis of differential transcript usage. *Genome Biol*. 2016;17(1):12.
28. Anders S, Reyes A, Huber W. Detecting differential usage of exons from RNA-seq data. *Genome Res*. 2012;22(10):2008–17.
29. Alexandrov LB, Nik-Zainal S, Wedge DC, Aparicio SA, Behjati S, Biankin AV, et al. Signatures of mutational processes in human cancer. *Nature*. 2013;500(7463):415.
30. Nik-Zainal S, Davies H, Staaf J, Ramakrishna M, Glodzik D, Zou X, et al. Landscape of somatic mutations in 560 breast cancer whole-genome sequences. *Nature*. 2016;534(7605):47.
31. R Core Team. R: a language and environment for statistical computing. Vienna, Austria; 2011. Available from: <https://www.R-project.org>.
32. Chen F. keleslab/surf. Surf. GitHub. 2020. Available from: <https://doi.org/10.5281/zenodo.3785574>.
33. Sammeth M, Foissac S, Guigó R. A general definition and nomenclature for alternative splicing events. *PLoS Comput Biol*. 2008;4(8):e1000147.
34. Benjamini Y, Hochberg Y. Controlling the false discovery rate: a practical and powerful approach to multiple testing. *J R Stat Soc Ser B Methodol*. 1995;57(1):289–300.
35. Aibar S, González-Blas CB, Moerman T, Imrichova H, Hulselmans G, Rambow F, et al. SCENIC: single-cell regulatory network inference and clustering. *Nat Methods*. 2017;14(11):1083.
36. Frankish A, Diekhans M, Ferreira AM, Johnson R, Jungreis I, Loveland J, et al. GENCODE reference annotation for the human and mouse genomes. *Nucleic Acids Res*. 2018;47(D1):D766–73.
37. Brooks AN, Duff MO, May G, Yang L, Bolisetty M, Landolin J, et al. Regulation of alternative splicing in *Drosophila* by 56 RNA binding proteins. *Genome Res*. 2015;25(11):1771–80.
38. Reyes A, Huber W. Alternative start and termination sites of transcription drive most transcript isoform differences across human tissues. *Nucleic Acids Res*. 2017;46(2):582–92.
39. Barash Y, Calarco JA, Gao W, Pan Q, Wang X, Shai O, et al. Deciphering the splicing code. *Nature*. 2010;465(7294):53.
40. Cáceres JF, Kornblihtt AR. Alternative splicing: multiple control mechanisms and involvement in human disease. *Trends Genet*. 2002;18(4):186–93.
41. Zhang X, Yan C, Zhan X, Li L, Lei J, Shi Y. Structure of the human activated spliceosome in three conformational states. *Cell Res*. 2018;28(3):307.
42. Sowd GA, Serrao E, Wang H, Wang W, Fadel HJ, Poeschla EM, et al. A critical role for alternative polyadenylation factor CPSF6 in targeting HIV-1 integration to transcriptionally active chromatin. *Proc Natl Acad Sci*. 2016;113(8):E1054–63.
43. Hentze MW, Castello A, Schwarzl T, Preiss T. A brave new world of RNA-binding proteins. *Nat Rev Mol Cell Biol*. 2018;19(5):327.
44. Xiong HY, Alipanahi B, Lee LJ, Bretschneider H, Merico D, Yuen RKC, et al. The human splicing code reveals new insights into the genetic determinants of disease. 2015;347(6218): <https://doi.org/10.1126/science.1254806>.
45. Jaganathan K, Panagiotopoulou SK, McRae JF, Darbandi SF, Knowles D, Li YI, et al. Predicting splicing from primary sequence with deep learning. *Cell*. 2019;176(3):535–48.
46. A deep neural network for predicting and engineering alternative polyadenylation. *Cell*. 2019;178(1):91–106.e23.
47. Bailey TL, Boden M, Buske FA, Frith M, Grant CE, Clementi L, et al. MEME SUITE: tools for motif discovery and searching. *Nucleic Acids Res*. 2009;37(suppl\_2):202–8.
48. Giudice G, Sánchez-Cabo F, Torroja C, Lara-Pezzi E. ATRACT—a database of RNA-binding proteins and associated motifs. *Database*. 2016. <https://doi.org/10.1093/database/baw035>.
49. Cienikova Z, Damberger FF, Hall J, Allain FHT, Maris C. Structural and mechanistic insights into poly (uridine) tract recognition by the hnRNP C RNA recognition motif. *J Am Chem Soc*. 2014;136(41):14536–44.
50. Dominguez D, Freese P, Alexis MS, Su A, Hochman M, Palden T, et al. Sequence, structure, and context preferences of human RNA binding proteins. *Mol Cell*. 2018;70(5):854–67.
51. Vejnar CE, Messih MA, Takacs CM, Yartseva V, Oikonomou P, Christiano R, et al. Genome wide analysis of 3' UTR sequence elements and proteins regulating mRNA stability during maternal-to-zygotic transition in zebrafish. *Genome Res*. 2019;29(7):1100–14.
52. Dember LM, Kim ND, Liu KQ, Anderson P. Individual RNA recognition motifs of TIA-1 and TIAR have different RNA binding specificities. *J Biol Chem*. 1996;271(5):2783–8.
53. Aznarez I, Barash Y, Shai O, He D, Zielenski J, Tsui LC, et al. A systematic analysis of intronic sequences downstream of 5' splice sites reveals a widespread role for U-rich motifs and TIA1/TIAL1 proteins in alternative splicing regulation. 2008;18(8):1247–58. <https://doi.org/10.1101/gr.073155.107>.
54. Wang I, Hennig J, Jagtap PKA, Sonntag M, Valcárcel J, Sattler M. Structure, dynamics and RNA binding of the multi-domain splicing factor TIA-1. *Nucleic Acids Res*. 2014;42(9):5949–66.
55. Legrand N, Dixon DA, Sobolewski C. AU-rich element-binding proteins in colorectal cancer. *World J Gastrointest Oncol*. 2019;11(2):71.
56. Martini A, La Starza R, Janssen H, Bilhou-Nabera C, Corveleyn A, Somers R, et al. Recurrent rearrangement of the Ewing's sarcoma gene, EWSR1, or its homologue, TAF15, with the transcription factor CIZ/NMP4 in acute leukemia. *Cancer Res*. 2002;62(19):5408–12.
57. Lukong KE, Chang Kw, Khandjian EW, Richard S. RNA-binding proteins in human genetic disease. *Trends Genet*. 2008;24(8):416–25.
58. Glisovic T, Bachorik JL, Yong J, Dreyfuss G. RNA-binding proteins and post-transcriptional gene regulation. *FEBS Lett*. 2008;582(14):1977–86.
59. Kim MY, Hur J, Jeong SJ. Emerging roles of RNA and RNA-binding protein network in cancer cells. *BMB Rep*. 2009;42(3):125–30.

60. Van Kouwenhove M, Kedde M, Agami R. MicroRNA regulation by RNA-binding proteins and its implications for cancer. *Nat Rev Cancer*. 2011;11(9):644.
61. King OD, Gitler AD, Shorter J. The tip of the iceberg: RNA-binding proteins with prion-like domains in neurodegenerative disease. *Brain Res*. 2012;1462:61–80.
62. Nussbacher JK, Batra R, Lagier-Tourenne C, Yeo GW. RNA-binding proteins in neurodegeneration: Seq and you shall receive. *Trends Neurosci*. 2015;38(4):226–36.
63. Seiler M, Peng S, Agrawal AA, Palacino J, Teng T, Zhu P, et al. Somatic mutational landscape of splicing factor genes and their functional consequences across 33 cancer types. *Cell Rep*. 2018;23(1):282–96.
64. Kahles A, Lehmann KV, Toussaint NC, Hüser M, Stark SG, Sachsenberg T, et al. Comprehensive analysis of alternative splicing across tumors from 8,705 patients. *Cancer Cell*. 2018;34(2):211–24.
65. Mayr C, Bartel D. Widespread shortening of 3'UTRs by alternative cleavage and polyadenylation activates oncogenes in cancer cells. *Cell*. 2009;138:673–84.
66. Yuan F, Hankey W, Wagner E, Li W, Wang Q. Alternative polyadenylation of mRNA and its role in cancer. *Genes Dis*. 2019;10:.
67. Qian J, Hassanein M, Hoeksema MD, Harris BK, Zou Y, Chen H, et al. The RNA binding protein FXR1 is a new driver in the 3q26-29 amplicon and predicts poor prognosis in human cancers. *Proc Natl Acad Sci*. 2015;112(11):3469–74.
68. Glasser E, Agrawal AA, Jenkins JL, Kielkopf CL. Cancer-associated mutations mapped on high-resolution structures of the U2AF2 RNA recognition motifs. *Biochemistry*. 2017;56(36):4757–61.
69. Zuo C, Shin S, Keleş S. atSNP: transcription factor binding affinity testing for regulatory SNP detection. *Bioinformatics*. 2015;31(20):3353–5.
70. Shin S, Hudson R, Harrison C, Craven M, Keleş S. atSNP Search: a web resource for statistically evaluating influence of human genetic variation on transcription factor binding. *Bioinformatics*. 2019;35(15):2657–9.
71. Li B, Dewey CN. RSEM: accurate transcript quantification from RNA-seq data with or without a reference genome. *BMC Bioinformatics*. 2011;12(1):323.
72. Liao Y, Smyth GK, Shi W. The R package Rsubread is easier, faster, cheaper and better for alignment and quantification of RNA sequencing reads. *Nucleic Acids Res*. 2019;47(8):e47.
73. Trapnell C, Hendrickson DG, Sauvageau M, Goff L, Rinn JL, Pachter L. Differential analysis of gene regulation at transcript resolution with RNA-seq. *Nat Biotechnol*. 2013;31(1):46.
74. Soneson C, Delorenzi M. A comparison of methods for differential expression analysis of RNA-seq data. *BMC Bioinformatics*. 2013;14(1):91.
75. Anders S, Huber W. Differential expression analysis for sequence count data. *Genome Biol*. 2010;11(10):R106.
76. Bailey TL, Elkan C. Fitting a mixture model by expectation maximization to discover motifs in bipolymers. In: *Proceedings of the Second International Conference on Intelligent Systems for Molecular Biology*. Menlo Park, California: AAAI Press; 1994. p. 28–36.
77. Roepcke S, Grossmann S, Rahmann S, Vingron M. T-Reg Comparator: an analysis tool for the comparison of position weight matrices. *Nucleic Acids Res*. 2005;33(suppl\_2):W438–41.
78. Murtagh F, Legendre P. Ward's hierarchical agglomerative clustering method: which algorithms implement Ward's criterion? *J Classif*. 2014;31(3):274–95.
79. Goldman M, Craft B, Hastie M, Repčeka K, McDade F, Kamath A, et al. The UCSC Xena platform for public and private cancer genomics data visualization and interpretation: Cold Spring Harbor Laboratory; 2019.
80. Chen F, Keleş S. Processed data and analysis results for 104 RBPs. Zenodo. 2020. Available from: <https://doi.org/10.5281/zenodo.3779037>.
81. Chen F. keleslab/surf-paper: ENCODE data analysis with SURF. GitHub. 2020. Available from: <https://doi.org/10.5281/zenodo.3785617>.

## Publisher's Note

Springer Nature remains neutral with regard to jurisdictional claims in published maps and institutional affiliations.

**Ready to submit your research? Choose BMC and benefit from:**

- fast, convenient online submission
- thorough peer review by experienced researchers in your field
- rapid publication on acceptance
- support for research data, including large and complex data types
- gold Open Access which fosters wider collaboration and increased citations
- maximum visibility for your research: over 100M website views per year

**At BMC, research is always in progress.**

Learn more [biomedcentral.com/submissions](https://biomedcentral.com/submissions)

